Accepted Manuscript

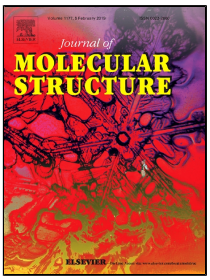

Synthesis, Characterization, Biological Screenings and Molecular Docking Study of Organotin(IV) Derivatives of 2,4-Dichlorophenoxyacetic Acid

Nida Naz, Muhammad Sirajuddin, Ali Haider, Syed Mustansar Abbas, Saqib Ali, Abdul Wadood, Mehreen Ghufran, Gauhar Rehman, Bushra Mirza

PII:	S0022-2860(18)31315-2
DOI:	10.1016/j.molstruc.2018.11.011
Reference:	MOLSTR 25840
To appear in:	*Journal of Molecular Structure*
Received Date:	16 October 2018
Accepted Date:	05 November 2018

Please cite this article as: Nida Naz, Muhammad Sirajuddin, Ali Haider, Syed Mustansar Abbas, Saqib Ali, Abdul Wadood, Mehreen Ghufran, Gauhar Rehman, Bushra Mirza, Synthesis, Characterization, Biological Screenings and Molecular Docking Study of Organotin(IV) Derivatives of 2,4-Dichlorophenoxyacetic Acid, *Journal of Molecular Structure* (2018), doi: 10.1016/j.molstruc.2018.11.011

Graphical Abstract: Pictogram

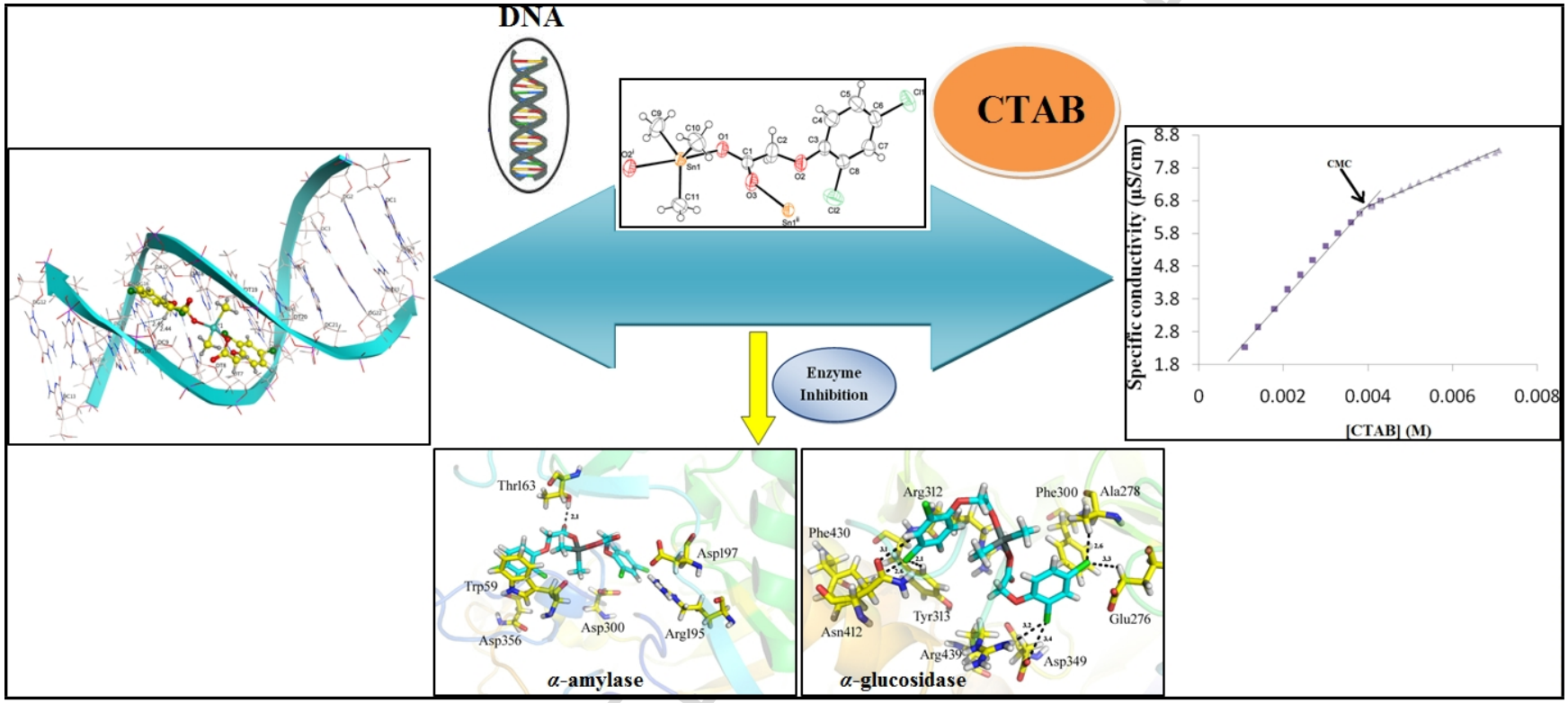

Synopsis for Graphical Abstract:

The novel organotin(IV) Carboxylates complexes interact with DNA *via* intercalative mode. Also they have strong tendency to interact with CTAB (surfactant) as indicated by higher CMC values and the resulting in micelle formation plays an important role in drug devilry. They show strong inhibitory potential against *α*-amylase and *α*-glucosidase. The DNA interaction and enzyme inhibition by Molecular Docking strongly support the experimental data.

Synthesis, Characterization, Biological Screenings and Molecular Docking Study of Organotin(IV) Derivatives of 2,4-Dichlorophenoxyacetic Acid

Nida Naz[a§], Muhammad Sirajuddin[b*§], Ali Haider[a*], Syed Mustansar Abbas[c,d], Saqib Ali[a], Abdul Wadood[e], Mehreen Ghufran[e], Gauhar Rehman[f], Bushra Mirza[f]

[a]Department of Chemistry, Quaid-i-Azam University Islamabad, 45320, Pakistan

[b]Department of Chemistry, University of Science and Technology Bannu, 28100, Pakistan

[c] Nanoscience & Technology Department, National Centre for Physics, Islamabad, Pakistan

[d] Department of Energy and Materials Engineering, Dongguk University, 30, Pildong-ro 1 gil, Jung-gu, Seoul 100-715, Republic of Korea

[e]Department of Biochemistry, Computational Medicinal Chemistry Laboratory, UCSS, Abdul Wali Khan University Mardan, Pakistan

[f]Department of Biochemistry, Quaid-i-Azam University Islamabad, 45320, Pakistan

[§]Authors Nida Naz and Muhmammad Sirajuddin Contributed equally

[*]Corresponding authors, e-mail: m.siraj09@yahoo.com (M. Sirajuddin); ahaider@qau.edu.pk (A. Haider)

Abstract

New tri- and diorganotin(IV) derivatives of 2,4-dichlorophenoxyacetic acid with general formula: R_3SnL and R_2SnL_2: {Me_3SnL (**1**), Bu_3SnL (**2**), Me_2SnL_2 (**3**), Bu_2SnL_2 (**4**) and Oct_2SnL_2 (**5**), L = 2,4-dichlorophenoxyacetate} have been synthesized and characterized in solid state by elemental and FT-IR analysis, whereas in solution state by ^{1}H- and ^{13}C-NMR spectroscopy. Compound **1** was also characterized by single crystal X-ray crystallography. The FT-IR data of compounds **1-5** confirm the bidentate binding mode of ligand with penta and hexa-coordinated arrangements around the Sn(IV) centre in solid state. The value of C-Sn-C angle for complexes **1** and **3** calculated from NMR (^{1}H and ^{13}C) data using Lockart's equation were 114.7° and 114.9°, respectively which falls in the range of 5-coordinated geometry. The DNA binding of synthesized compounds were studied *via* UV-Vis spectroscopy and viscometry resulting in an intercalative mode of interaction. Molecular docking analysis of the studied compounds also supports the results of the UV-vis and viscometry. Moreover, interaction of the synthesized compounds with a cationic surfactant i.e., cetyltrimethyl ammonium bromide (CTAB) has been studied by conductometric method. Enzyme inhibition activity against α-amylase and α-

glucosidase was carried out and compound **3** was found to possess maximum inhibition (88.1% and 91.3%, respectively). The theoretical study also enforce the experimental data for enzyme inhibition of the compound **3** (docking score = -12.4096) by forming seven hydrogen bonds and two pi-H linkages with the Glu 276, Ala 278, Phe 300, Arg 312, Tyr 313, Asp 349, Asn 412, Phe 430 and Arg 439 residues of the binding pocket of the α-glucosidase. The potency of the compound **3** might be due to the presence of the strong electron withdrawing chloro group. IC_{50} value of the brine shrimp activity revealed that triorganotin(IV) derivatives (**1** and **2**) were more toxic than their diorganotin(IV) analogues. Moreover, compound **2** has the MIC values of 12.5 µg/mL and 6.25 µg/mL against *S. Aureus* and *M. Leuteus* bacterial strains, respectively.

Keywords: Organotin(IV) derivative; DNA interaction study; Cetyltrimethyl ammonium bromide (CTAB); Enzyme inhibition activity; Molecular docking

1. Introduction

Organotins are intensively used organometallic compounds worldwide (~ 50,000 t yr^{-1}) with applications in the stabilization of plastics, precursors in glass coating and as antifungal agents in textiles and other household's items [1]. From the 1950s-2001, tributyltin (TBT), dibutyltin (DBT), monobutyltin (MBT) and triphenyltin (TPhT) compounds are the most widely used active ingredients in marine antifouling coating to resist the settlement of biofouling agents [2]. Despite the environmental and toxicological problems associated with the technological use of organotin compounds [3], they are among the most widely employed organometallic species and continue to surprise experts in the field of medicinal inorganic chemistry [4, 5].

Organotin compounds of the general formula R_nSnX_{4-n} display a wide range of biological effects depending on the ligand X, its number n and on the type of the organic group R bound to the metal ion [6, 7]. The organotin(IV) compounds have been widely investigated during the last few decades because of their potential antibacterial and anticancer activities [8]. It is noticeable that some organotin(IV) complexes showed higher *in vitro* cytotoxic activities than *cis*-platin [9]. Therefore, the synthesis of novel organotin complexes and the investigation of their biological activities are of great importance [10].

Among the organotin compounds, organotin carboxylates are important from for biological point of view as they possess broad applications in medicine [11]. Many of the diorganotin and triorganotin compounds possess intriguing molecular structures such as ladder, O-capped cube,

butterfly, drum, football cage, cyclic trimer and so on that resulted in promising applications. The structure of organotin carboxylates can be tuned by the ligand type, reaction conditions and the organotin groups [12]. In order to understand the regulation of synthesis and the structural-biomedical application relation much attention has been paid on the preparation, characterization and biological activities of organotin carboxylates against tumour cells, fungi, bacteria and other microorganisms [13,14]. Nowadays, resistance of microorganisms and toxicity are some of the major problems concerning the clinical use of drugs. Therefore, the search for new metal-containing antimicrobial agents, more bio-specific and less toxic to the host and to the environment, is particularly important. In the continuation of our work on organotin(IV) carboxylates, herein, we report on the synthesis and spectroscopic studies of di- and triorganotin(IV) derivatives of 2,4-dichlorophenoxyacetic acid. These complexes are investigated for their DNA binding and screened for enzyme inhibition and microbial activity. Moreover, we have studied their interactions with cationic surfactant, i.e., CTAB by conductometric method.

2. Experimental

2.1. Materials and methods

The organotin(IV) chlorides and oxide were purchased from Aldrich, USA and were used without further purification. The solvents used were procured from E. Merck, Germany and dried before use by the reported method [15]. The melting points were measured in a capillary tube by using the Gallenkamp (UK) electro thermal melting point apparatus. The FT-IR spectra were recorded on a Thermo Nicolet-6700 FT-IR Spectrophotometer in the range of 4000-400 cm^{-1}. The ^{1}H- and ^{13}C-NMR were recorded at room temperature in deuterated solvents on a Bruker Advance Digital 300 MHz FT-NMR spectrometer. Elemental analyses were done using a CE-440 Elemental Analyzer (Exeter Analytical, Inc). DNA binding studies were performed using Ubbelohde viscometer and double beam spectrophotometer UV-1601 from Shimadzu, Japan. The interaction of the synthesized compounds with CTAB was studied using ELICO (type CM 82T) bridge equipped with platinized electrodes (cell constant = 1.02 cm^{-1}) conductometer.

2.2. General procedure for the Synthesis of NaL and Organotin(IV) derivatives

The NaL was prepared by stirring a mixture of equimolar amount of sodium hydrogen carbonate (dissolved in distilled water) with 2,4-dichlorophenoxyacetic acid (suspended in distilled water).

The mixture was stirred for 30 minutes to get the clear solution. The solvent was rotary evaporated to get the desired product (Scheme 1) [16].

Triorganotin(IV) derivatives (**1** and **2**) were synthesized by refluxing the mixture of equimolar NaL (5 mmol) and R_3SnL {R = CH_3 (**1**), *n*-C_4H_9 (**2**)} (5 mmol) in dried toluene for 6-7 h (scheme 1) [16]. It was then cooled to room temperature and filtered. The filtrate was rotary evaporated to obtain the desired product which was recrystallized in chloroform and *n*-hexane (4:1 ratio).

Diorganotin(IV) derivatives (**3** and **4**) were synthesized by the same procedure [16] as used for the triorganotin(IV) derivatives with the only difference of molar ratio: NaL (10 mmol) and R_2SnCl_2 (5 mmol) (scheme 1).

Complex **5** was synthesized by refluxing the mixture of 2,4-dichlorophenoxyacetic acid (10 mmol) and $(C_8H_{17})_2SnO$ (5 mmol) in dried toluene using the Dean and Stark apparatus, for 6-7 h and water formed during the reaction was removed (scheme 1).

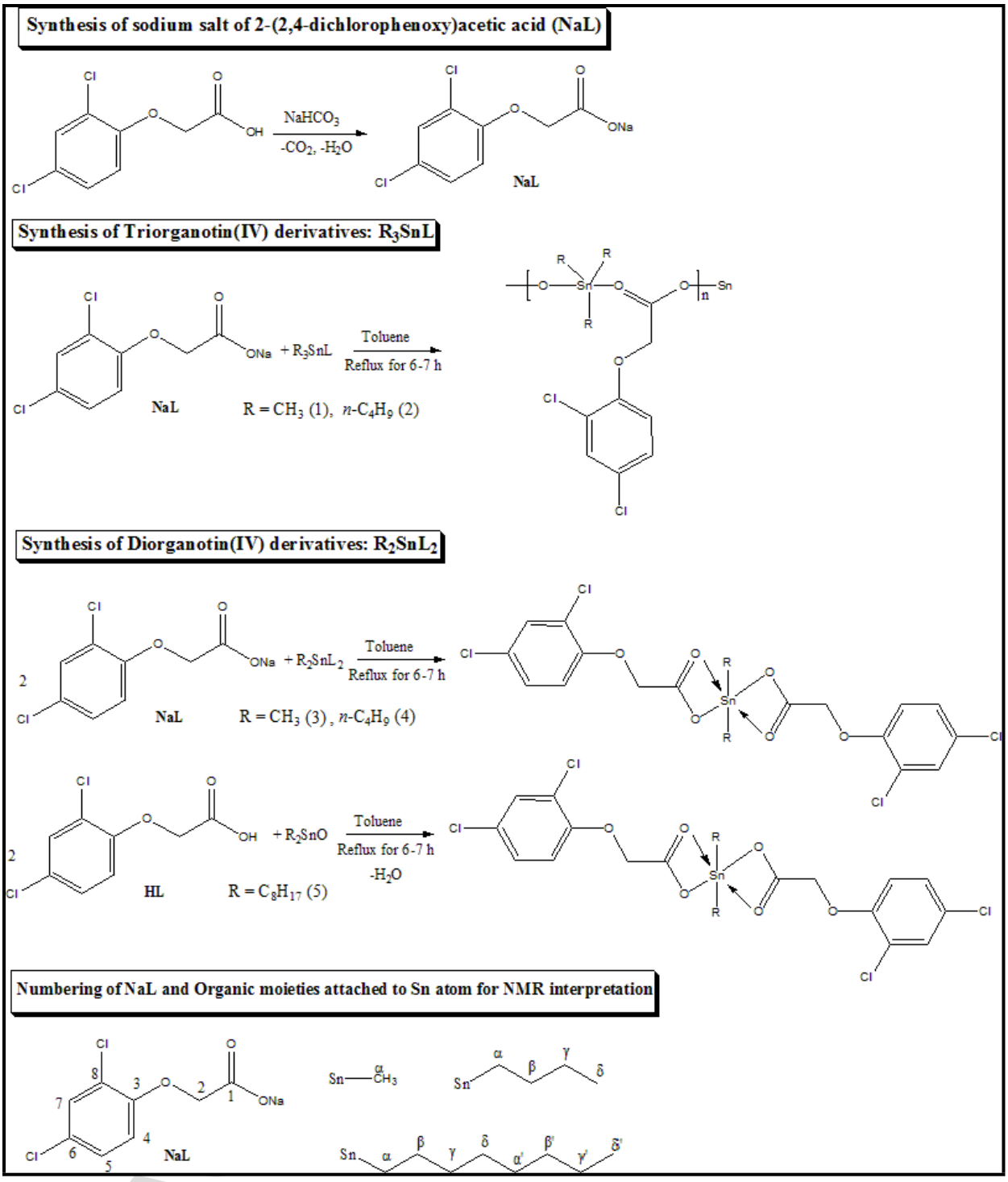

Scheme 1: Synthetic pathway for NaL and its Organotin(IV) derivatives

2.2. DNA interaction study

2.2.1. UV–visible spectroscopy

SS-DNA (20 mg) was dissolved in deionized water (pH = 7.0) by stirring for overnight and stored at 4°C. 20 mM Phosphate buffer (NaH_2PO_4–Na_2HPO_4, pH = 7.2) was prepared in distilled water. A solution of SS-DNA in 20 mM Phosphate buffer gave a ratio of UV absorbance at 260 and 280 nm (A_{260}/A_{280}) of 1.8 which confirms that DNA is free from proteins [17-20]. The molar absorption coefficient 6600 $M^{-1}cm^{-1}$ (260 nm) was used to find concentration of SS-DNA which was 1.4 x 10^{-4} M. The 1 mM complex was dissolved in 60% DMSO. Keeping the complex concentration constant and the SS-DNA concentration varying the UV absorption titrations were made. The SS-DNA solution of equal amount was added to the reference and complex to get rid of absorbance of DNA itself. Before taking measurements compound-DNA solutions were incubate for about 10 min at 25 °C. Using 1 cm path length cuvettes absorption spectra were recorded [17-20].

2.2.2. Viscosity measurements

Ubbelodhe viscometer was used to determine the viscosity at a room temperature using a digital stopwatch. The flow time of sample was measured in triplicate and the average was taken. The viscosity data were plotted as $(\eta/\eta_o)^{1/3}$ *vs.* binding ratio (r) of [Compound]/[DNA]. Where η is the relative viscosity of DNA in the presence of compounds, η_o is the relative viscosity of DNA only. Viscosity values were calculated from the observed flow time of DNA containing solutions corrected for the flow time of 20 mM phosphate buffer solution (pH 7.2) alone. The viscosity for DNA in the presence and absence of the compound was calculated from the following equations [21]:

$$\eta_o = t - t_o \quad \text{and} \quad \eta = \frac{t - t_o}{t_o}$$

2.3. CTAB Interaction study

The interaction of synthesized compounds with CTAB was investigated by conductometric method. The measurements were performed on an ELICO (type CM 82T) bridge equipped with platinized electrodes (cell constant =1.02 cm^{-1}). The conductivity runs were carried out by adding concentrated CTAB stock solution progressively into the thermostated solvent (dimineralized double-distilled water of specific conductivity (1-2 × 10^{-6} Scm^{-1}) at 30 °C. The

critical micellar concentration of the pure CTAB was obtained from the plots of specific conductivity as a function of the CTAB concentration. The CMC values were taken from the intersection of the two straight lines drawn before and after the intersection point versus surfactant concentration plots [22].

2.4. *In vitro* bioactivities

2.4.1. Brine shrimp cytotoxicity assay

Brine shrimp cytotoxicity assay was used to determine the toxicity of the compounds [23, 24]. *Artemia salina* (brine shrimp) eggs (Ocean Star Inc., USA) were hatched in seawater (34 gL^{-1}). After 24 h, ten shrimps were transferred to each vial using Pasteur pipette. The compounds with final concentrations of 400, 200, 100, 50, 10, and 5 μgmL^{-1} were added and the volume was raised up to 5 mL adding artificial seawater. Vincristine sulphate was used as positive control and DMSO was used as negative control. The experiments were performed in triplicate and vials were incubated under illumination at 28 °C. After 24 h, survivors were counted and IC_{50} (lethal concentration) values were calculated by using the Finney software.

2.4.2. Antibacterial activity

The *in vitro* antibacterial evaluation of the synthesized compounds was performed using the disc diffusion method [25]. In experiment two gram positive: *Staphylococcus aureus* (ATCC 6538) and *Micrococcus luteus* (ATCC 10240) and two gram negative: *Escherichia coli* (ATCC 15224) and *Enterobacter aerogens* (ATCC 13048) were cultured in nutrient broth for 24h at 37 °C. These cultured strains were used as inoculums (1%) to run the assay. Each bacterial strain was added to the nutrient agar medium at 45 °C, poured into sterile Petri plates and allowed to solidify. 5 mL of the test compound with final concentration of 200 mg/mL was poured on sterile filter paper discs (4 mm) and placed on nutrient ager plates, respectively. Kanamycin and DMSO were used as positive and negative controls, respectively on each plate. The assay was performed in triplicate and the plates were incubated at 37 °C for 24–48 h. The antibacterial activity of the compounds was determined by measuring the diameter of zones showing complete inhibition (mm) with the help of vernier caliper.

2.4.3. Antifungal assay

The *in vitro* antifungal evaluation of the synthesized compounds was performed using the disc diffusion method [25] against the following fungal strains: *Mucor species* (FCBP 0300),

Aspergillus niger (FCBP 0198) and *Aspergillus fumigates* (FCBP-066). Sabouraud dextrose agar (SDA) was used to culture the fungal strains at 28°C for 5 to 7 days. Actively growing fungal spores of each strain were spread with the help of autoclaved cotton swaps on solidified SDA Petri plates under sterile conditions. The compounds (5 mL of each final concentration of 200 mg/mL) were transferred on sterile filter paper discs (4 mm) and placed on SDA plates. Terbinafine and DMSO served as positive and negative controls, respectively on each plate. All plates were incubated at 28 °C for 5 to 7 days and with the help of vernier caliper the fungal growth was measured (mm).

2.4.4. α-Amylase inhibition assay

The compounds were tested for their enzyme inhibition activity against α-amylase by the previously reported method [26]. For assay 5 µL of each test compound with the final concentration of 400 µg/mL was mixed with 40 µL of starch (0.05 %) and 30 µL of potassium phosphate buffer (pH 6.8) in 96-well micro titer plates followed by the addition of 10 µL of α-amylase enzyme (0.2 U/well). Acarbose and DMSO were used as positive and negative control, respectively. The plates were incubated for 30 min at 50 °C and 20 µL HCl (1M) as stopping reagent was added. Then 100 µL of iodine reagent (5 mM KI and 5 mM I_2) was added to check the presence and absence of starch and absorbance was measured at 540 nm with microplate reader (Bio Tek, Elx800, USA). The experiments were performed in triplicate and percent inhibition was calculated.

2.4.5. α-Glucosidase inhibition assay

p-Nitrophenyl-α-D-glucopyranoside, Acarbose and Baker's Yeast alpha glucosidase were purchased from Sigma (USA). The alpha glucosidase was dissolved in 100 mM phosphate buffer (pH 6.8) and was used as the enzyme extract. *p*-Nitrophenyl-α-D-glucopyranoside was used as the substrate. Organotin compounds were used in the concentration of 400 µg/mL. Compounds were mixed with 320 µL of 100 mM phosphate buffer (pH 6.8) at 30 °C for 5 minutes. Sodium hydroxide (3 mL of 50 mM) was added to the mixture and the absorbance was read at 410 nm. The control samples were prepared without any compound. Acarbose was used as the reference alpha glucosidase inhibitor [27-29]. All tests were performed in triplicate. The percentage was determined by mean of inhibitory values.

2.4.6. Molecular docking

Docking is a significant tool to explore the interactions between an inhibitor and the target [30]. To find the binding interactions of these compounds in the active sites DNA, α-glucosidase and α-amylase, the MOE-Dock program was used to perform molecular docking. The crystal structure of α-glucosidase is not available yet, so, we used homology model as described by Ming Liu *et al*., [31] while the 3D crystal structure of the α-amylase (1HNY) and DNA (1BNA) were retrieved from the Protein Databank (PDB). The structures of the derivatives were built in MOE (www.chemcomp.com) and energy minimized using the default parameters of the MOE. The DNA, α-glucosidase and α-amylase were allowed to dock to the compounds using MOE by the default parameters i.e., Placement: Triangle Matcher, Rescoring: London dG. For each ligand ten conformations were generated. The top-ranked conformation of each compound was used for further analysis.

3. Results and discussion

All the compounds were synthesized in good yield and their melting point along with other physical data are given in Table 1.

Table 1: Physical data of the synthesized organotin(IV) derivatives 1-5[a]

Comp. No	% Yield	M.P	M. Formula	M. Wt	Elemental analyses data (%) Calculated (Found)	
					C	H
1	73	89-90	$C_{11}H_{14}Cl_2O_3Sn$	383.84	34.42 (34.02)	3.68 (3.87)
2	76	158-160	$C_{20}H_{32}Cl_2O_3Sn$	510.08	47.09 (47.87)	6.32 (6.99)
3	63	143-145	$C_{16}H_{18}Cl_4O_6Sn$	566.84	33.90 (33.71)	3.20 (3.11)
4	69	177-179	$C_{24}H_{28}Cl_4O_6Sn$	673	42.83 (42.25)	4.19 (4.25)
5	82	163-165	$C_{32}H_{44}Cl_4O_6Sn$	785.21	48.95 (49.01)	5.65 (5.55)

a) Numbering of compounds is according to Scheme 1.

3.1. FT-IR spectra

From FT-IR data in Table 2, the absence of broad peak for acidic -OH, shifting of two C=O bands (asymmetric and symmetric) and appearance of two new peaks for Sn-C and Sn-O in the range of 540-575 cm^{-1} and 440-485 cm^{-1}, respectively confirms the synthesis of complexes **1-5**.

According to Deacon and Phillips, Δν for monodentate bonding increases compared to the free anion; for bidentate chelating Δν decreases; and, for bidentate bridging, Δν remains similar to the free anion [32]. The values of Δν are calculated as: $\Delta\nu = \nu COO_{asym} - \nu COO_{sym}$ and indicate the bidendate binding mode of the COO^- moiety around the Sn atom in the present series of compounds.

Table 2: FT-IR data ν (cm^{-1}) of HL, NaL and its organotin(IV) derivatives 1-5[a]

Comp. No	ν(O-H)	νCOO_{asym}	νCOO_{sym}	$\Delta\nu(\nu COO_{asym} - \nu COO_{sym})$	νSn-C	νSn-O
HL	3420	1667	1421	246	-	-
NaL	-	1638	1443	195	-	-
1	-	1508	1347	161	546	439
2	-	1523	1370	153	542	487
3	-	1509	1374	135	563	437
4	-	1506	1375	131	566	479
5	-	1513	1379	134	535	453

a) Numbering of compounds is according to Scheme 1.

3.2. NMR spectroscopy

3.2.1. ^{1}H-NMR

Compounds **1** and **3** which contain the methyl protons bonded to tin metal exhibited a definite singlet at 0.71 ppm and 0.89 ppm having ^2J ($^{119/117}$Sn-^{1}H) values of 65 and 98 Hz, respectively. The ^2J values fall in the range of the 5-and 6-coordinated trigonal bipyradial and octahedral geometries around the tin atom for tri- and di-organotin(IV) derivatives, respectively [4]. In compounds **2, 4** and **5** the terminal methyl protons of butyl and octyl groups bonded to tin atom gave a triplet each whereas all the rest of protons show multiplets. All the proton signals for ligand are observed at same positions after complexation except those which are close to the COO group show slightly downfield shift because of ligand to metal charge transfer which further confirmed the complex formation. The ^{1}H NMR values of all the synthesized complexes are given in the Table 3.

Table 3: ^{1}H NMR data (ppm) of organotin(IV) derivatives 1-5[a]

Comp. No	OH (s, 1H)	H2 (s, 2H)	H4 (d, 1H)	H5 (d, 1H)	H7 (s, 1H)	Sn-H
HL	11.01	4.26	6.86-6.82	7.27-7.23	7.48	-
1	-	4.66	6.75-6.72	7.18-7.15	7.31	0.71 (s, 9H, H_α), $^{2}J[^{1}H\text{-}^{119}Sn]$ = 65 Hz C-Sn-C = 114.9°
2	-	4.66	6.75-6.72	7.16-7.12	7.39	3H (t)0.84-0.8, 2H (t)1.01-1.46 4H (m)1.23-1.30
3	-	4.77	6.81-6.78	7.21-7.18	7.41	0.89 (s, 9H, H_α), $^{2}J[^{1}H\text{-}^{119}Sn]$ = 98 Hz, C-Sn-C = 145°
4	-	4.77	6.78-6.75	7.19-7.15	7.42	Sn-$(C_4H_9)_2$ 0.02-1.76 (m)
5	-	4.76	6.78-6.75	7.19-7.15	7.42	Sn-C_8H_{17} 0.02-1.84 (m)

a) Numbering of compounds is according to Scheme 1.

3.2.2. ^{13}C NMR

All complexes have clearly been characterized by ^{13}C-NMR, where the appearance of characteristic peaks of alkyl groups around the tin centre that were absent in the free ligand spectrum and the downfield shift of the peak of carbonyl carbon confirms the assimilation of organotin moiety (Table 4). In ^{13}C-NMR of compounds **1** and **3**, the coupling constants for satellites due to $^{1}J[^{119/117}Sn\text{-}^{13}C]$ coupling, have been calculated to be 432 Hz and 776 Hz, respectively that corresponds to the θ(C-Sn-C) value of 114.7° and 144.8°, respectively by applying Lockhart's equation. The θ values suggest a 5-coordination geometry for triorganotin(IV) derivatives and a 6-coordination geometry for diorganotin(IV) derivatives, respectively in solution [33].

Table 4: ^{13}C NMR data of HL and its organotin(IV) derivatives 1-5[a]

Comp. No	C1	C2	C3	C4	C5	C6	C7	C8	Sn-C
HL	170.5	68.6	154.2	115.6	127.1	127.9	129.2	122.2	-
1	172.6	66.6	152.0	114.1	126.4	127.4	130.2	123.9	-4.6 (C_α), $^1J[^{13}C\text{-}^{119}Sn]$ = 432 Hz, C-Sn-C = 114.7°
2	172.4	65.4	152.7	114.3	126.3	127.6	130.4	123.7	17.6 (C_α), 25.4 (C_β), 24.7 (C_γ), 13.2 (C_δ)
3	175.1	66.0	152.1	114.5	127.4	128.5	130.5	124.2	1.05 (C_α), $^1J[^{13}C\text{-}^{119}Sn]$ = 776 Hz, C-Sn-C = 144.8°
4	177.2	66.3	152.3	114.4	127.0	127.4	130.5	124.2	18.6 (C_α), 26.4 (C_β), 25.9 (C_γ),13.6 (C_δ)
5	177.2	66.3	152.3	114.3	127.6	127.4	130.5	124.2	14.1-33.3 ($C_{\alpha\text{-}\delta'}$)

a) Numbering of compounds is according to Scheme 1.

3.3. Crystal structure of compound 1

Crystal structure of compound **1** is shown in Figure 1 whereas crystal data and structural refinement parameters are given in Table 5. The selected bond lengths and bond angles are reported in Table 6. The data reveals that the compound **1** adopted monoclinic crystal system with $P2_1/c$ space group. The carboxylate ligand coordinates with two Sn(IV) atoms in a bridging mode. The geometry around the Sn atom is distorted trigonal bipyramidal, wherein three methyl groups are bonded to the Sn atom at equatorial positions with almost identical bond distances [mean Sn-C = 2.113 Å] and two O atoms of the carboxylate ligand are bonded asymmetrically with significantly different Sn-O distances of 2.198 Å and 2.468 Å [34]. The C-Sn-C bond angles (C9-Sn1-C10, C10-Sn1-C11, C9-Sn1-C11) are 114.92°, 125.06° and 119.19°, respectively and their sum is 359.17°. The O1-Sn1-O2 bond angle is 171.58°. The slight distortion is due to

the asymmetrically bonded carboxylate ligands. The τ value (τ = (β-α)/60, where β is the largest basal angle around the tin atom while α is the next largest angle around the tin atom) is 0.94 that falls in the range of 5-coornidated distorted trigonal bipyramidal geometry [16, 34]. Packing diagram of complex is shown in Figure 2.

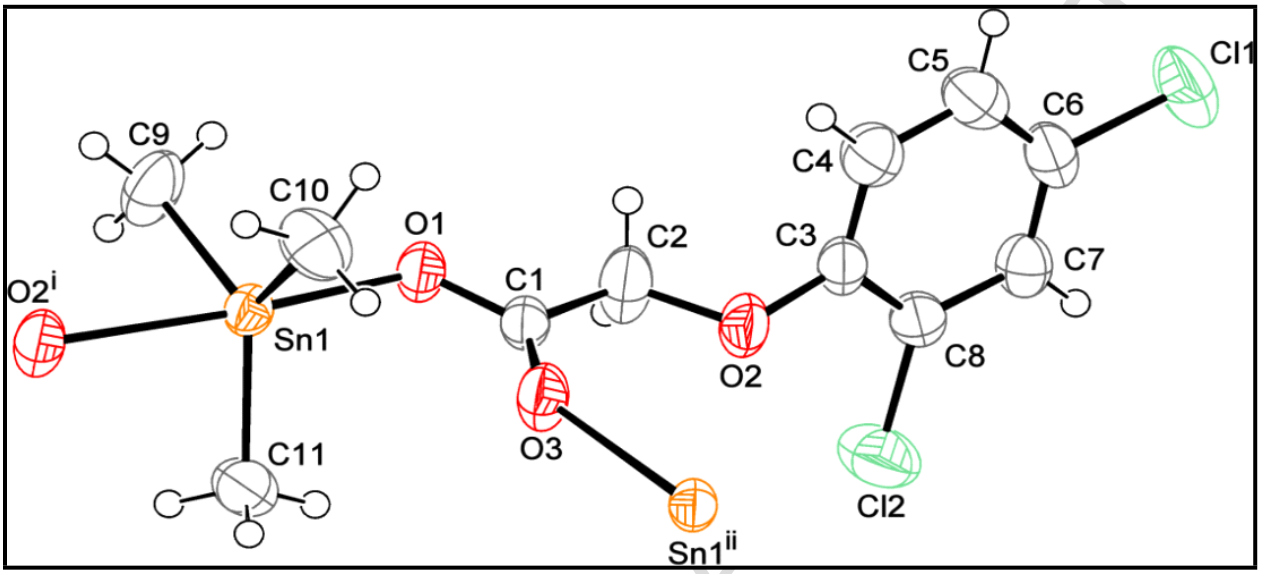

Figure 1: The asymmetric unit of complex **1** with displacement ellipsoids drawn at the 50% probability level. Symmetry codes: (i) -x, 1/2+y, 1/2-z; (ii) -x, -1/2+y, 1/2-z.

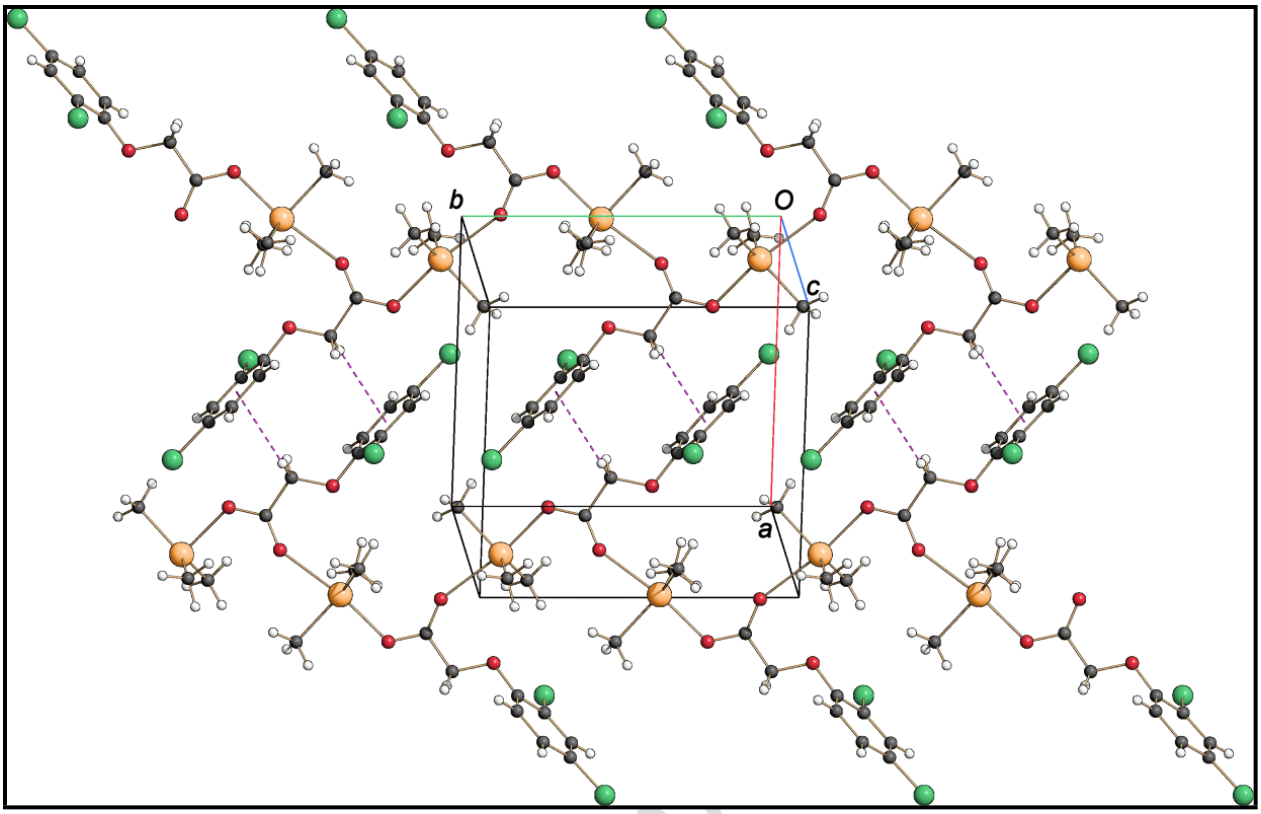

Figure 2: Crystal packing structure of complex **1** Packing showing the formation of polymeric one-dimensional chains parallel to the *b* axis. C-H...π interactions linking chains into layers parallel to the (-1 0 2) plane are shown as dashed lines.

Table 5: Crystal data and structure refinement for complex 1

Empirical formula	$C_{11}H_{14}Cl_2O_3Sn$
Formula weight	383.81
Temperature/K	294(2)
Crystal system	monoclinic
Space group	$P2_1/c$
a, b, c /Å	10.6125(6), 10.4869(6), 13.5397(8)
α, β, γ /°	90, 104.0598(8), 90
Volume/Å^3	1461.72(15)
Z	4
ρ_{calc}g/cm^3	1.744
μ/mm^{-1}	2.107
F(000)	752.0
Crystal size/mm^3	0.320 × 0.280 × 0.200
Radiation	MoKα (λ = 0.71073)
2θ range for data collection/°	3.956 to 50.994
Index ranges	$-12 \le h \le 12$, $-12 \le k \le 12$, $-16 \le l \le 16$
Reflections collected	15751
Independent reflections	2711 [R_{int} = 0.0285, R_{sigma} = 0.0183]
Data/restraints/parameters	2711/0/157
Goodness-of-fit on F^2	1.122
Final R indexes [I>=2σ (I)]	R_1 = 0.0230, wR_2 = 0.0573
Final R indexes [all data]	R_1 = 0.0238, wR_2 = 0.0577
Largest diff. peak/hole / e Å^{-3}	0.27/-0.73
CCDC	1823040

Table 5: Selected bond angles (°) and bond lengths (Å) for complex 1

Selected bond angles							
Atom	**Atom**	**Atom**	**Bond Angle**	**Atom**	**Atom**	**Atom**	**Bond Angle**
O1	Sn1	O2	171.58(6)	C11	Sn1	O1	94.71(10)
C9	Sn1	O1	88.99(10)	C11	Sn1	O2	86.06(10)
C9	Sn1	O2	83.34(10)	C11	Sn1	C9	119.19(15)
C10	Sn1	O1	95.02(10)	C11	Sn1	C10	125.06(14)
C10	Sn1	O2	91.38(11)	C1	O1	Sn1	123.35(15)
C10	Sn1	C9	114.92(15)	C1	O2	Sn1	148.25(16)

Selected Bond lengths					
Atom	**Atom**	**Bond lengths (Å)**	**Atom**	**Atom**	**Bond lengths (Å)**
Sn1	O1	2.198(17)	O2	Sn1	2.463(18)
Sn1	O2	2.463(18)	O2	C1	1.221(3)
Sn1	C9	2.122(3)	O3	C3	1.376(3)
Sn1	C10	2.110(3)	C1	C2	1.508(4)
Sn1	C11	2.108(3)	C3	C4	1.381(4)
Cl1	C6	1.740(3)	C3	C8	1.382(4)
Cl2	C8	1.727(3)	O1	C1	1.277(3)

3.4. DNA interaction studies

3.4.1. UV-Visible spectroscopy

The absorption spectrum was initially used to study the interaction between the SS-DNA and the synthesized complexes. Figures 3 and 4 represent the representative complexes interaction with different concentrations of DNA. It was observed that the synthesized compounds show one strong absorption peak in the range of 267-286 nm which is due to the π-π* transitions of aromatic ring [35]. With the increasing concentrations of DNA, hypochromic along with minor bathochromic shift was observed in the spectrum of the free compound peak which is the sign of intercalation. In the intercalation mode of interaction, the drug insertion occurs between the two strands of DNA which is generally adopted by the polycyclic or aromatic ring having planar structures due to resemblance with DNA bases [35]. After the intercalation, the π* orbital of

intercalated molecule interacts with the π orbital of the base pairs thus reduction of π-π* transition occur resulting in bathochromic effect, which support the intercalative mode of interaction. At λ_{max} reduction in the absorbance appears as a result of π-π* transition which was used to measure DNA binding constant K (M^{-1}) from the intercept of graph plotted between $A_o/(A-A_o)$ *vs* 1/[DNA]. High drug-DNA interaction in the range of 10^3 to 10^4 was found for all the synthesized complexes. For di- and triorganotin(IV) complexes UV-Vis absorption studies were carried out and the results of binding constant values (Table 6) confirm that triorganotin(IV) derivatives show higher values of binding constants than their diorganotin(IV) because of more lipophillic character of triorganotin(IV) derivatives. Based on the variation in absorbance, the binding constant of this complex with DNA was determined according to Benesi-Hildebrand equation [36].

$$\frac{A_0}{A-A_0} = \frac{\varepsilon_G}{\varepsilon_{H-G}-\varepsilon_G} \times \frac{1}{K[DNA]} + \frac{\varepsilon_G}{\varepsilon_{H-G}-\varepsilon_G}$$

Where *K* is the binding constant, A_o and *A* are the absorbances of the drug and its complex with DNA, respectively, and ε_G and ε_{H-G} are the absorption coefficients of the drug and the drug-DNA complex, respectively. The association constant was obtained from the intercept-to-slope ratios of $A_o/(A-A_o)$ *vs*. 1/[DNA] plot.

K = c/m x 10^6 (c = intercept = $\frac{\varepsilon_G}{\varepsilon_{H-G}-\varepsilon_G}$ and m = slope = $\frac{\varepsilon_G}{\varepsilon_{H-G}-\varepsilon_G}$) (for binding constant)

ΔG = -RT ln*K* (R = 8.314 J/mol, T = 298K) (for Gibb's Free energy, ΔG)

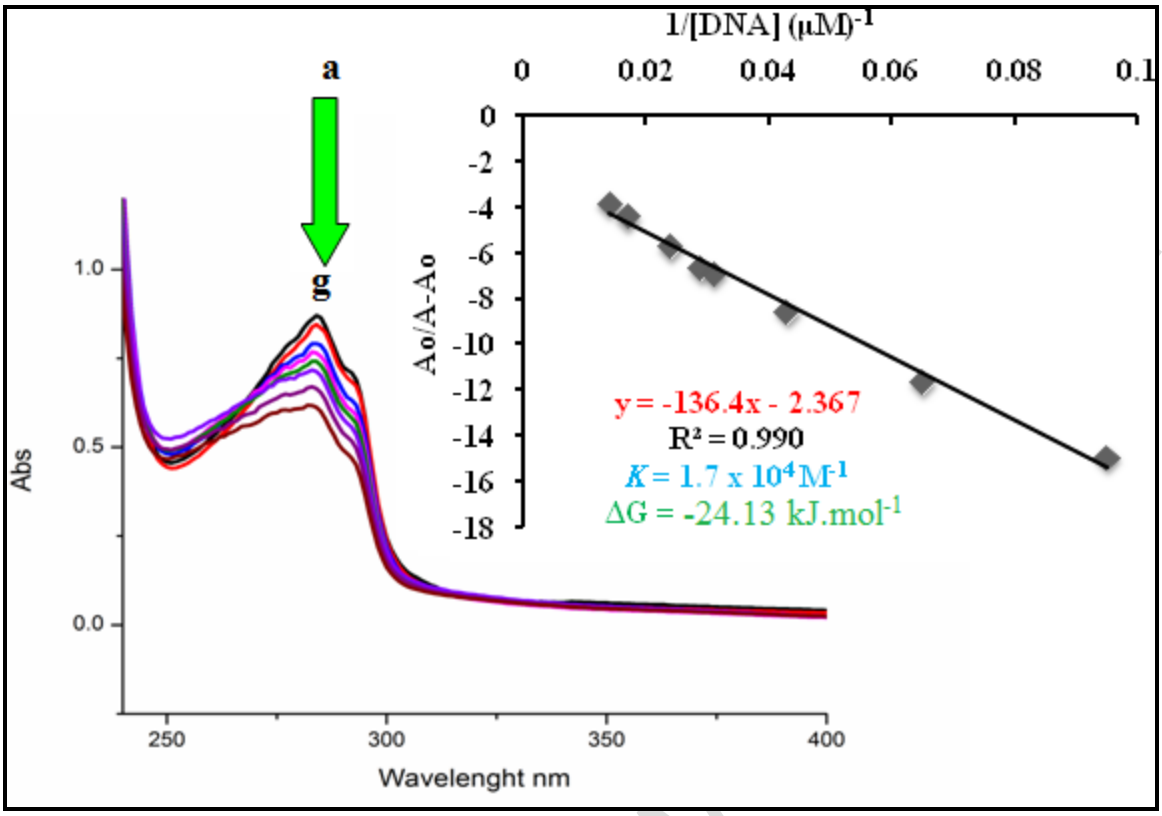

Figure 3: Absorption spectrum of 2 mM of complex **1** in the absence and presence of 5 to 35 μM of DNA. The arrow direction indicates increasing concentrations of DNA. The inset graph represents the plot of $A_o/A\text{-}A_o$ *vs*. 1/[DNA] $(\mu M)^{-1}$ for the calculation of binding constant (*K*) and Gibb's free energy (ΔG).

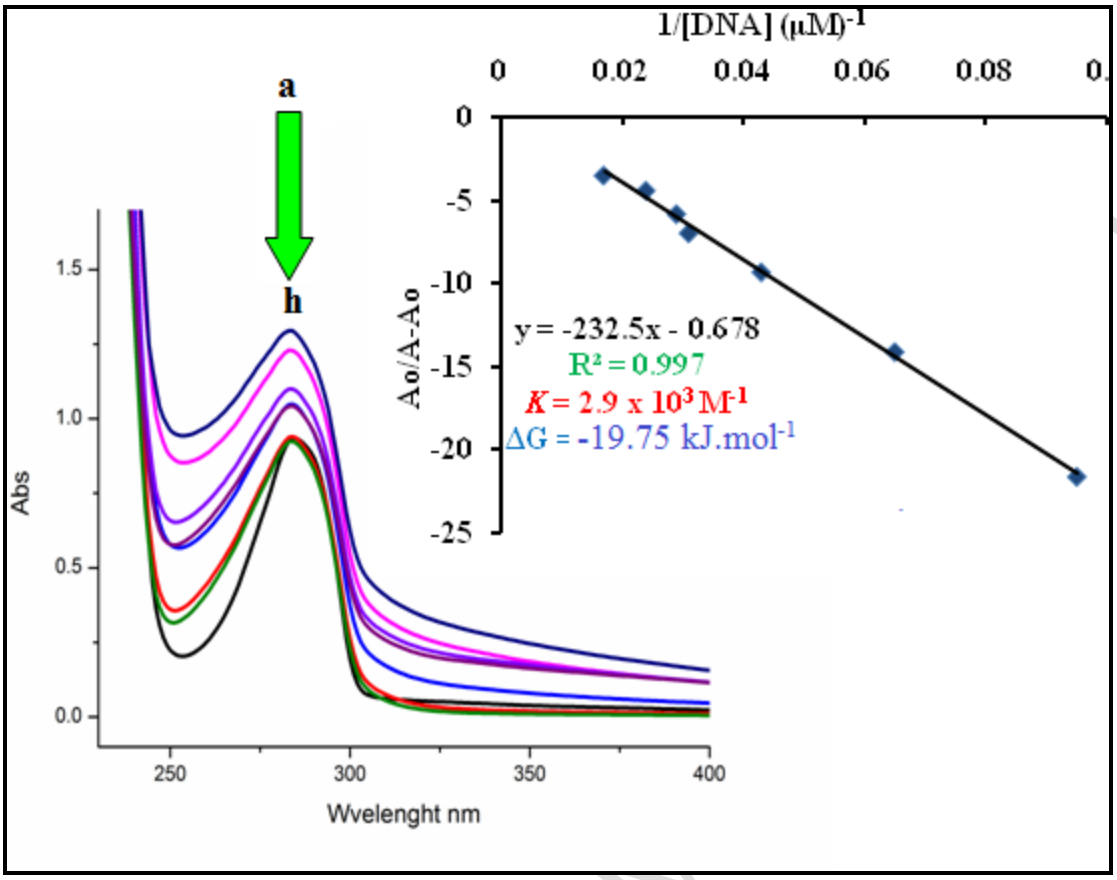

Figure 4: Absorption spectrum of 2 mM of complex **5** in the absence and presence of 5 to 35 µM of DNA. The arrow direction indicates increasing concentrations of DNA. The inset graph represents the plot of $A_o/A\text{-}A_o$ *vs*. 1/[DNA] $(\mu M)^{-1}$ for the calculation of binding constant (*K*) and Gibb's free energy (ΔG).

Table 6: Binding constant (K) and Gibb's free energy (ΔG) values calculated from UV-Vis. for organotin(IV) derivatives 1-5[a]

Comp. No	K (M^{-1})	ΔG ($kJ.Mol^{-1}$)
1	1.7×10^4	-24.13
2	2.03×10^4	-24.57
3	3.21×10^3	-20.00
4	6.41×10^3	-21.72
5	2.9×10^3	-19.75

Numbering of compounds is according to Scheme 1.

3.4.2. Viscometry

Viscometric technique was used to further conform the binding mode of the synthesized compounds with SS-DNA. The concentration of the compounds was kept constant while that of the DNA was varied. The relative viscosity $(\eta/\eta_0)^{1/3}$ was plotted *vs.* concentration ratio of drug-DNA adduct as shown in Figure 5 for the representative compounds. The intercalative mode was favored when increase in viscosity was observed because when the drug interacts with DNA bases the attractive forces between the DNA bases turn out to be weak and conformational changes take place with increase in the torsional angle and finally the length of DNA increases by uncoiling the two strand of DNA [37]. In terms of time flow the relative viscosity also increases due to the increase in DNA length.

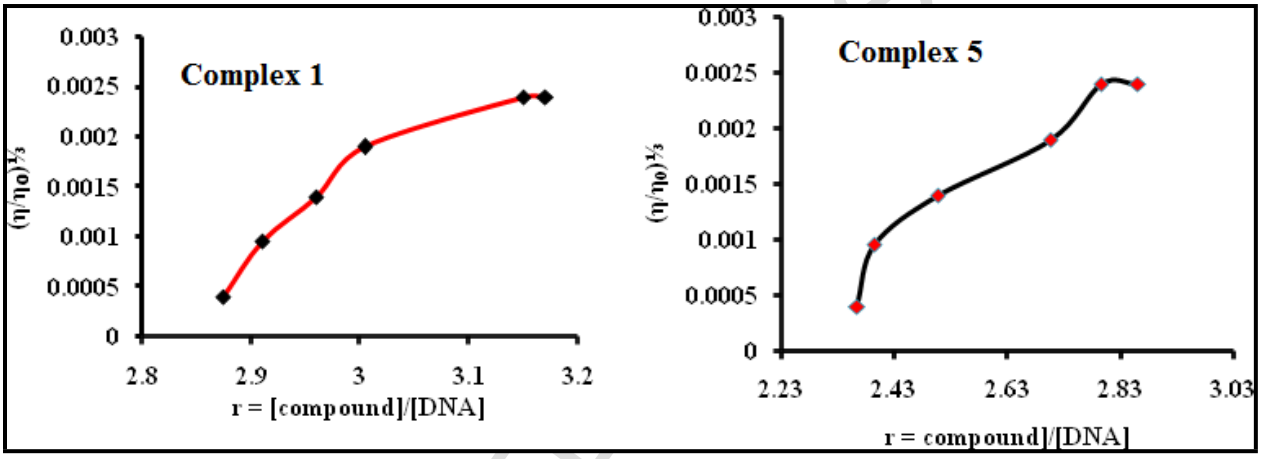

Figure 5: Effects of increasing amount of representative complexes **1** and **5** on relative viscosity of DNA at 25±1 °C. [DNA] = 2.37×10^{-5} M.

3.5. Interaction with CTAB

The specific conductance of synthesized organotin (IV) complexes (1mM) with CTAB (0-0.007 M) were recorded to study the complex–CTAB interactions. The data of conductance were plotted against the CTAB concentration used as shown in Figure 6 which shows that by increasing the CTAB concentration the conductance increases and at 0.0039 M CTAB concentration, an inflection point was observed which is the point at which CTAB monomers combine to shape a structure called micelle. That inflection point is known as critical micelle concentration (CMC) of CTAB. By adding the CTAB, the $CTAB^+$ and Br^- ions were formed which reduced the surface tension of aqueous media so increases the conductance [38]. The conductance was observed to be sharply increase in the pre-micellar concentration region while

the free monomers were used to form micelle in post-micellar concentration thus lowered the speed of increase in conductance [39]. When the complex was present then the CTAB CMC value was observed at high concentration as compared to its aqueous solution because the complex molecules strongly bind to the $CTAB^+$ monomers. On interaction of complex molecules, the repulsion between $CTAB^+$ monomers decreases by reducing its charge density.

ΔG_m is the free energy for the micellisation process which can be calculated by the equation

$$\Delta G_m = 2.303(1+\beta)\, RT\log X_{cmc}$$

where β = the degree of the counter ion binding and

$$\beta = 1-\alpha$$

α is the extent of dissociation or ionization which is calculated before and after CMC from the ratio of plots.

$$\alpha = S_2/S_1$$

cmc is taken in mole fractions called as X_{cmc} which in aqueous solution can be calculated as

$$X_{cmc} = cmc/55.55$$

ΔG_m and CMC for the complexes are given in Table 7, the variation of G values at highest concentration and in the absence of surfactant is the ΔG_m and its negative value indicate instinctive solubilization of compound in micelle because of attractive forces between the compound and positively charged micelle results in stable CTAB-complex system. Specific conductance data for the complexes in presence of CTAB (0–0.007M) were recorded to measure complex–CTAB interaction parameters.

Table 7: CMC and Gibb's free energy (ΔG) values of selected organotin(IV) derivatives 1-4[a]

Comp. No	CMC value	ΔG value (kJ.mol^{-1})
1	0.0039	-38.5
2	0.0028	-34.2
3	0.0015	-39.4
4	0.0013	-32.5

Numbering of compounds is according to Scheme 1.

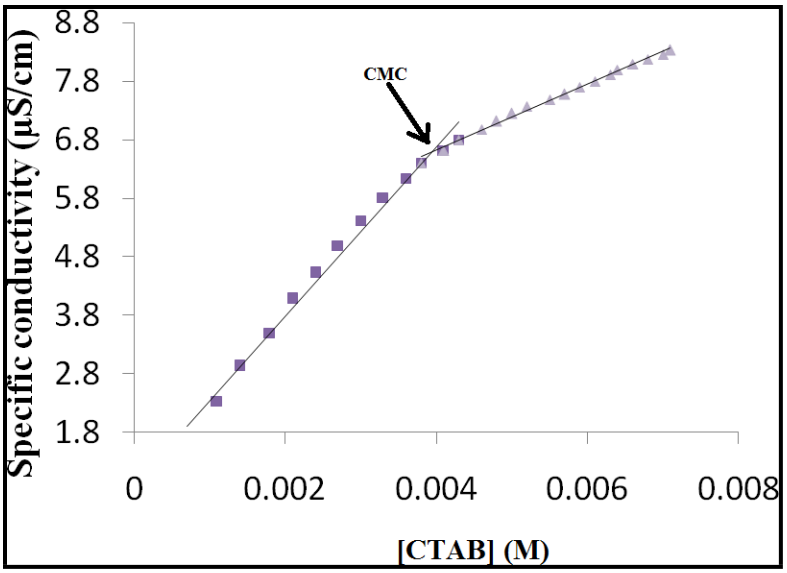

Figure 6: Specific conductivity curves of CTAB in the presence of the complex **1** in water

3.7. *In vitro* Biological evaluation

3.7.1. Antibacterial activity

All the synthesized compounds were screened for *in vitro* antibacterial activity against four bacterial strains including two Gram positive (*Staphylococcus aureus and Micrococcus luteus)* and two Gram negative strains *(Enterobacter aerogenes and Escherichia coli)* using agar disc diffusion method. The synthesized compounds were dissolved in DMSO at concentration of 400 µg/mL. The results showed that most of the compounds were active against all the strains. Compounds **2**, **3** and **4** were most potent showing activity against most of the tested strains**.** Further compound Bu_3SnL has shown outstanding activity against *M. leuteus* showing maximum zone of inhibition 53.0 mm. Bu_2SnL_2 compound was found active against all the tested bacterial strains. The results of all the compounds are summarized in the Tables 8 and 9.

Table 8: Antibacterial activity data of HL and its organotin(IV) derivatives 1-5[a]

Comp. No.	Zone of inhibition in mm (Conc. 400 µg/mL)			
	E. coli	*E. aerogenes*	*S. aureus*	*M. leuteus*
HL	-	-	-	-
1	12.4	-	-	-
2	6.3	-	7.4	53.0
3	7	-	-	11.0
4	9.1	12.5	9.4	11.4
5	-	-	-	-
Kanamycine[b]	21.2	22.4	23.1	24.6

a) Numbering of compounds is according to Scheme 1. b) Standard drug

Table 9: Minimum inhibitory concentration (MIC) of HL and its organotin(IV) derivatives 1-5[a]

Comp. No.	MIC (µg/mL)			
	E. coli	*E. aerogenes*	*S. aureus*	*M. leuteus*
HL	-	-	-	-
1	200	-	200	-
2	25	200	12.5	6.25
3	100	-	200	100
4	50	200	50	100
5	-	-	-	-

a) Numbering of compounds is according to Scheme 1.

3.7.2. Antifungal activity

The synthesized compounds were subjected to *in vitro* antifungal activity against three fungal strains *(Mucor species, A. niger* and *Aspergillus fumigatus)* using the disk dilution method [29]. Turbinafine was used as the standered drug. All the compounds, except HL, **3** and **5** have shown antifungal activity against the various strains. Compound **2** shows higher activity than the reference drug against *M. mucor*. Data of the antifungal activity is shown in Table 10.

Table 10: Zone of inhibition (mm) of antifungal activity of HL and its organotin(IV) derivatives 1-5[a]

Comp. No	Zone of inhibition in mm (Conc. 400 µg/mL)		
	A. fumigates	***A. niger***	***M. specie***
HL	-	-	-
1	15.4	13.1	10.7
2	21.2	-	23.6
3	-	-	9.0
4	8.1	8.3	6.2
5	-	-	-
Terbinafine[b]	28.6	26.4	21.0

a) Numbering of compounds is according to Scheme 1. b) Standard drug

3.7.3. Cytotoxicity

To screen out the biologically active compounds, brine shrimp cytotoxicity assay was performed and results are summarized in Table 10. Brine shrimp cytotoxicity assay serves as predictive test for the identification of bioactive compounds to evaluate anticancer potential of any compound. All the tested compounds are highly cytotoxic with IC_{50} value as low as 0.69 μgmL^{-1} (Table 10). It is important to note that these compounds are more potent than the vincristine sulphate (positive control) which means that these compounds have strong potential for the anticancer screening. Compounds **1-4** had shown moderate level of lethality. Compound **5** was found totally lethal against the shrimps.

Table 10: Brine shrimp cytotoxicity data of HL and its organotin(IV) derivatives 1-5[a]

Comp. No.	Percent mortality after 24 h at different concentrations (µg/mL)						IC_{50}
	400	200	100	50	10	5	
HL	70	55	50	40	35	10	9.81
1	100	100	100	100	60	40	0.69
2	100	100	100	100	50	40	0.81
3	100	100	100	100	40	30	1.07
4	100	100	80	70	45	30	1.38
5	50	50	50	45	25	15	18.83

a) Numbering of compounds is according to Scheme 1.

3.7.4. α-Amylase assay

The compounds were evaluated for their enzyme inhibition potential against α-amylase enzyme and results in the form of percentage values as given in Table 12. Experiment was performed in triplicates and acarbose was used as a positive control. The results showed that the only compound **3** exhibited enzyme inhibition activity with percentage value of 88.1 and other compounds were found inactive.

3.7.5. α-Glucosidase inhibition activity

α-glucosidase inhibition assay was performed on all test compounds. Among the tested compound all the compounds except compound **5** showed inhibition activity. Compounds **2** and **3** showed superb inhibition activity. Rest of the compounds showed moderate activity. Results of alpha glucosidase inhibition assay are given in Table 12.

Table 12: % inhibition of alpha amylase and alpha glucosidase inhibition of HL and its organotin(IV) derivatives 1-5[a]

Comp. No	α-amylase (% inhibition)	α-glucosidase (% inhibition)
HL	7.1	87.4
1	7.8	67.7
2	11.2	76.6
3	88.1	91.3
4	6.4	83.0
5	10.5	41.9

a) Numbering of compounds is according to Scheme 1.

3.8. Docking analysis of DNA

To explore the binding mode of these derivatives, molecular docking was performed. The docking results showed that all the metal-complex derivatives bind to DNA by intercalation, which is the only interaction mode we obtained by docking. From the docking conformation of the most active compound, compound **3** (docking score = -12.2325), it was observed that this compound established two H-donor interactions with active site residues DC 9 and DG 10 of DNA respectively as well as four pi-H linkages with the DT 7, DT 8, DC 9 and DG 10 residues of the DNA (Figure **7**). An excellent arrangement was obtained as the best docked pose showed important binding features mostly based on interactions due to various interacting moieties of derivatives, and phosphorus atom including its versatile structural features.

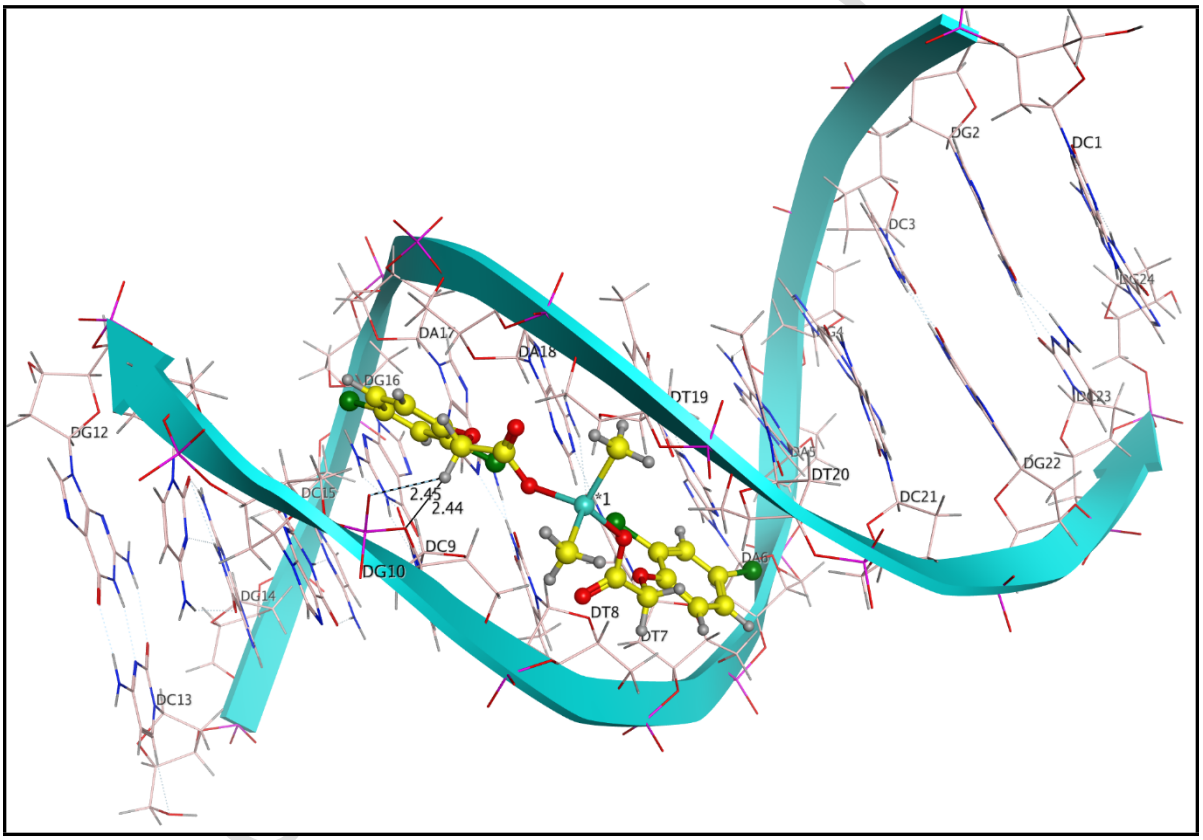

Figure 7: Docking orientation of **3** inside the active site of DNA.

3.9. Docking analysis of α-Glucosidase and α-Amylase

The docking results of the compounds with the α-amylase and α-glucosidase enzymes have given good information about the nature of the binding mode that was excellent correlated with

the experimental results. Compound **3** is the most active compound with highest docking score (-10.8071) as well as inhibitory activity (88.1% inhibition). Compound **3** is bound to the α-amylase in an adequate manner through one H-acceptor interaction and pi-pi interactions with the active site residues Thr 163 and Trp 59 (Figure 8). The reason of the good activity of the ligand **3** could be accredited to this strong binding with amino acid residues through polar interaction as well as metal ligation. From the molecular docking studies, it was observed that the top ranked conformation of all the compounds fit well inside the active site of the homology model of α-glucosidase (Glu276, Asp 349 and Arg439) [40]. From the docking conformation of the compounds, it was revealed that compound **3** (% inhibition 91.3, docking score = -12.4096) formed seven hydrogen bonds and two pi-H linkages with the Glu 276, Ala 278, Phe 300, Arg 312, Tyr 313, Asp 349, Asn 412, Phe 430 and Arg 439 residues of the binding pocket of the α-glucosidase as shown in Figure 9. The potency of the compound **3** might be due to the presence of the strong electron withdrawing group (-Cl).

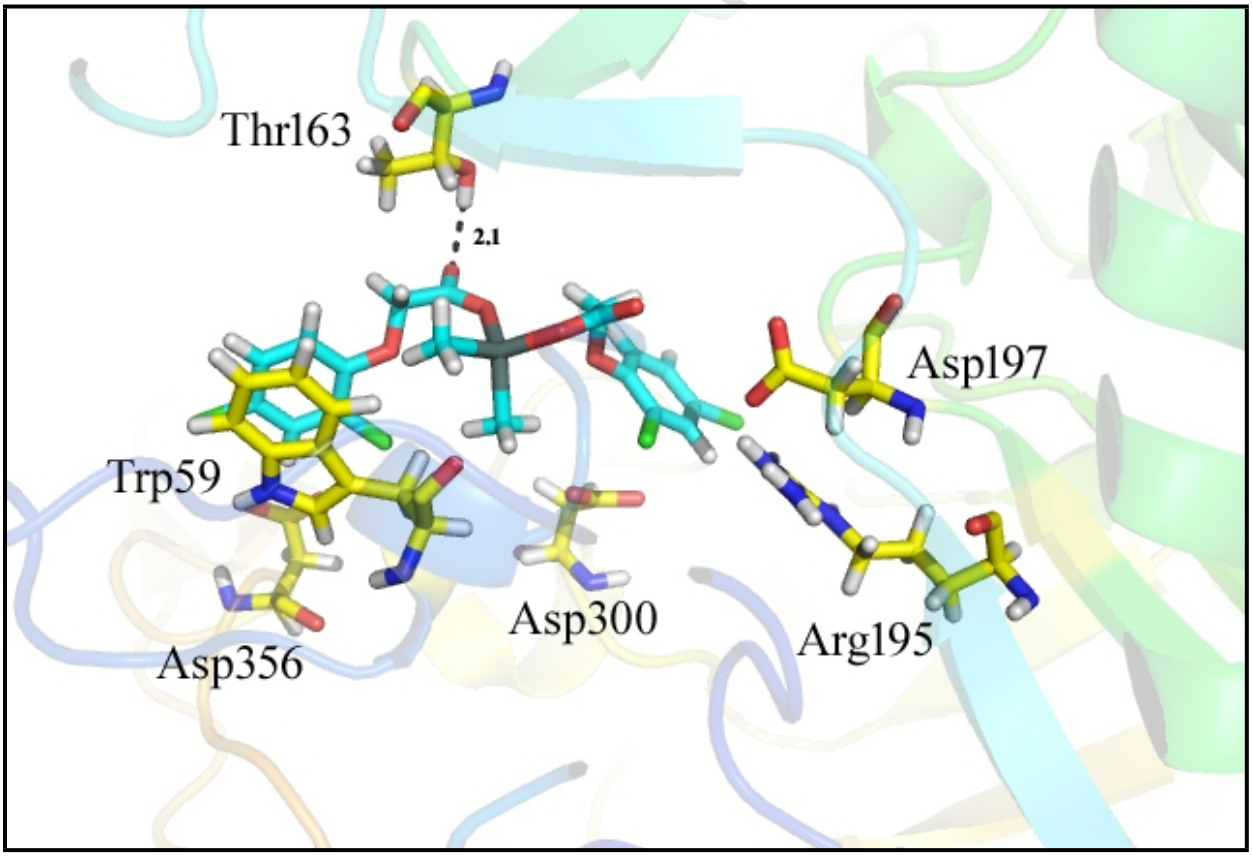

Figure 8: Docking conformation of compound **3** in the active site of *α*-amylase.

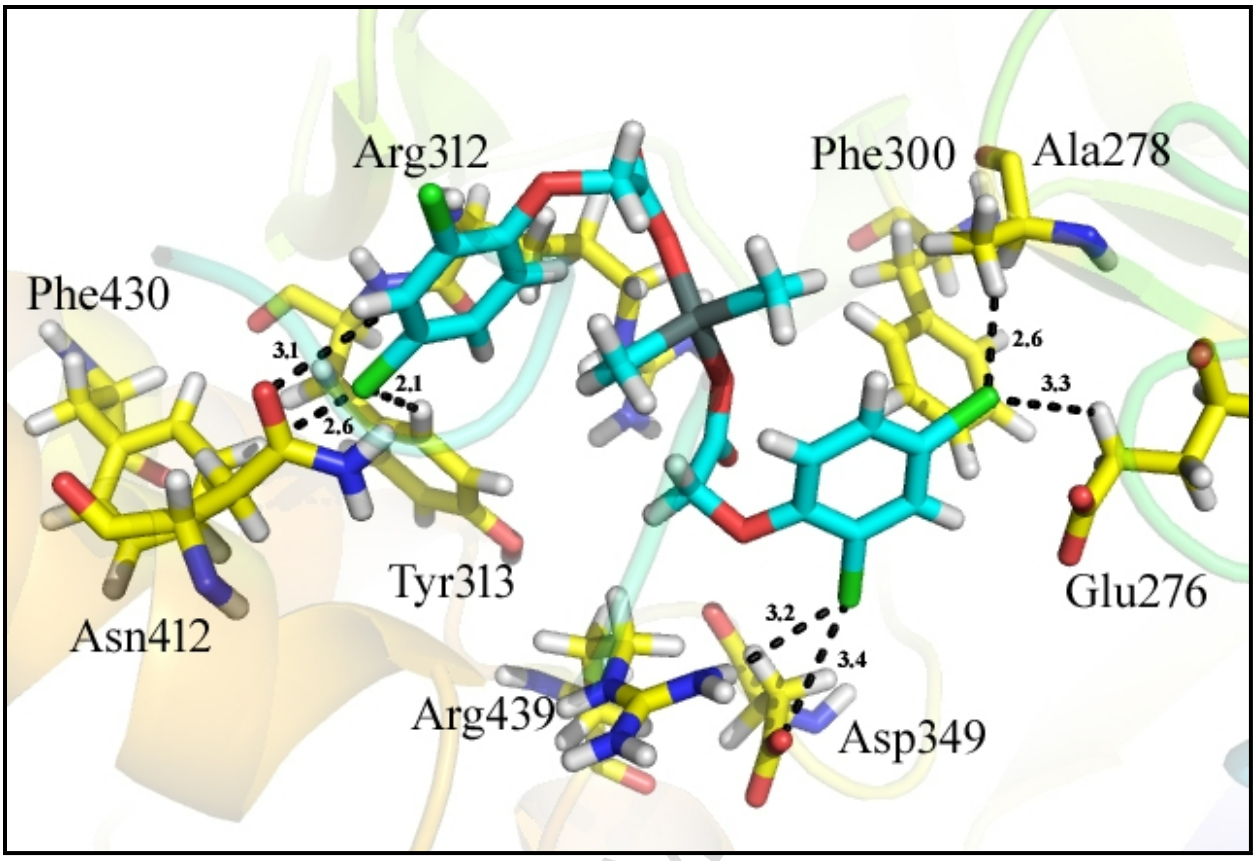

Figure 9: Docking conformation of compound **3** in the active site of α-glucosidase.

Conclusions

New di- and triorganotin(IV) complexes of oxygen donor ligand have been synthesized in quantitative yields. The appearance of new peaks for Sn-O and disappearance of O-H peaks of acidic OH in the FT-IR spectra indicated the formation of organotin(IV) complexes. Multinuclear NMR (^{1}H and ^{13}C) data further confirmed the formation of complexes. Compound **1** was also analyzed by X-ray single crystal analysis which revealed polymeric type bridged trigonal bipyramidal structure with bidentate bridging mode of the carboxylate moiety. For SSD DNA-Complex binding studies, the decrease in the absorbance (UV-Visible) and increase in the relative viscosity supports the intercalative mode of interaction for the screened compounds. Moreover, in case of complex-CTAB interactions, the higher value of CMC supports the idea of high binding capability of organotin-withCTAB micelles due to electrostatic interations while the negative value of energy changes suggests the spontaneous nature of transfer of organotin molecules from bulk water to CTAB micelle. Biological studies of the compounds reveal that triorganotin(IV) derivatives have higher activity than the corresponding diorganotin(IV), perhaps

due to their greater lipophilicity and permeability through the cell membrane. The high lipid solubility of organotin compounds ensures cell penetration and association with intracellular sites. The promising cytotoxicity results of the synthesized compounds show that they may represent a new series of antitumor agents for the prevention and treatment of cancer. These compounds also present strong inhibition against different enzymes like alpha amylase and alpha glucosidase.

Acknowledgment

M. Sirajuddin (Pin# P7-017) gratefully acknowledges the Higher Education Commission (HEC) Islamabad, Pakistan, for financial support.

References

[1] R.F. Cole, G.A. Mills, M.S. Hale, R. Parker, T. Bolam, P.R. Teasdaled, W.W. Bennett, G.R. Fones, Development and evaluation of a new diffusive gradients in thin-films technique for measuring organotin compounds in coastal sediment pore water, Talanta 178 (2018) 670-678.

[2] S.K. Sarkar, Organotin Compounds in Surface Sediments of Sundarban Wetland and Adjacent Coastal Regions, Trace Metals in a Tropical Mangrove Wetland, 2018, pp 173-187.

[3] A.C.A. Sousa, M.R. Pastorinho, S. Takahashi, S. Tanabe, History on organotin compounds, from snails to humans, Environ. Chem. Lett., 12 (2014) 117-137.

[4] M. Sirajuddin, S. Ali, V. Mckee, M. Sohail, H. Pasha, Potentially bioactive organotin(IV) compounds: synthesis, characterization, in vitro bioactivities and interaction with SS-DNA, Eur. J. Med. Chem. 84 (2014) 343-363.

[5] F. Arjmand, M. Muddassir, I. Yousuf, Design and synthesis of enantiomeric (R)-and (S)-copper (II) and diorganotin (IV)-based antitumor agents: Their in vitro DNA binding profile, cleavage efficiency and cytotoxicity studies, J. Photochem. Photobiol., B 136 (2014) 62-71.

[6] E. Katsoulakou, M. Tiliakos, G. Papaefstathiou, A. Terzis, C. Raptopoulou, G. Geromichalos, K. Papazisis, R. Papi, A. Pantazaki, D. Kyriakidis,, Diorganotin (IV) complexes of dipeptides containing the α-aminoisobutyryl residue (Aib): Preparation, structural characterization, antibacterial and antiproliferative activities of [$(n\text{-}Bu)_2Sn$ (H_{-1}

L)] (LH= H-Aib-L-Leu-OH, H-Aib-L-Ala-OH). J. Inorg. Biochem., 102 (2008) 1397-1405.

[7] M. Sirajuddin, S. Ali, A. Haider, N.A. Shah, A. Shah, M.R. Khan, Synthesis, characterization, biological screenings and interaction with calf thymus DNA as well as electrochemical studies of adducts formed by azomethine [2-((3,5-dimethylphenylimino)methyl)phenol] and organotin(IV) chlorides Polyhedron 40 (2012) 19-31.

[8] M. Sirajuddin, V. McKee, M. Tariq, S. Ali, Newly designed organotin(IV) carboxylates with peptide linkage: Synthesis, structural elucidation, physicochemical characterizations and pharmacological investigations, Eur. J. Med. Chem., 143 (2018) 1903-1918.

[9] M. Hong, G.L. Chang, R. Li, M.J. Niu, Anti-proliferative activity and DNA/BSA interactions of five mono- or di-organotin(IV) compounds derived from 2-hydroxy-N'-[(2-hydroxy-3-methoxyphenyl)methylidene]-benzohydrazone, New J. Chem., 40 (2016) 7889-7900.

[10] K. Liu, H. Yan, G. Chang, Z. Li, M. Niu, M. Hong, Organotin(IV) complexes derived from hydrazone Schiff base: synthesis, crystal structure, in vitro cytotoxicity and DNA/BSA interactions, Inorgan. Chim. Acta, 464 (2017) 137-146.

[11] A. Gianguzza, O. Giuffre, D. Piazzese, S. Sammartano, Aqueous solution chemistry of alkyltin(IV) compounds for speciation studies in biological fluids and natural waters, Coord. Chem. Rev., 256 (2012) 222-239.

[12] X. Xiao, J. Liang, J. Xie, X. Liu, D. Zhu, Y. Dong, Organotin(IV) carboxylates based on 2-(1,3-dioxo-1H-benzo[de]isoquinolin-2(3H)-yl)acetic acid: syntheses, crystal structures, luminescent properties and antitumor activities, J. Mol. Struc., 1146 (2017) 233-241.

[13] H. Tlahuext, R. Reyes-Martinez, G. Vargas-Pineda, M. Lopez-Cardoso, H. Hopfl, Molecular structures and supramolecular association of chlorodiorganotin (IV) complexes with bis-and tris-dithiocarbamate ligand, J. Organomet. Chem., 696 (2011) 693-701.

[14] A. Normah, K.N. Farahana, B. Ester, H. Asmah, N. Rajab, A.A. Halim, Cytotoxic and genotoxic effect of triphenyltin (IV) benzylisopropyldithiocarbamate in thymoma murine cell line (WEHI 7.2), Res. J. Chem. Environ., 15 (2011) 544-549.

[15] W.L.F. Armarego, C.L.L. Chai, Purification of Laboratory Chemicals, fifth ed., Butterworth-Heinemann, London, New York, 2003.

[16] M. Sirajuddin, S. Ali, V. McKee, S. Zaib, J. Iqbal, Organotin (IV) carboxylate derivatives as a new addition to anticancer and antileishmanial agents: design, physicochemical characterization and interaction with Salmon sperm DNA, RSC Adv., 4 (2014) 57505–57521.

[17] M. Sirajuddin, S. Ali, V. McKee, H. Ullah, Synthesis, spectroscopic characterization and in vitro antimicrobial, anticancer and antileishmanial activities as well interaction with Salmon sperm DNA of newly synthesized carboxylic acid derivative, 4-(4-methoxy-2-nitrophenylamino)-4-oxobutanoic acid, Spectrochim. Acta Part A, 138 (2015) 569–578.

[18] A. Abbas, S. Murtaza, M.N. Tahir, S. Shamim, M. Sirajuddin, U.A. Rana, K. Naseem, H. Rafique, Synthesis, antioxidant, enzyme inhibition and DNA binding studies of novel N-benzylated derivatives of sulfonamide, J. Mol. Struc., 1117 (2016) 269-275.

[19] N. Uddin, M. Sirajuddin, N. Uddin, M. Tariq, H. Ullah, S. Ali, S.A. Tirmizi, A.R. Khan, Synthesis, spectroscopic characterization, biological screenings, DNA binding study and POM analyses of transition metal carboxylates, Spectrochim. Acta Part A, 140 (2015) 563-574.

[20] S. Murtaza, S. Shamim, N. Kousar, M.N. Tahir, M. Sirajuddin, U.A. Rana, Synthesis, biological investigation, calf thymus DNA binding and docking studies of the sulfonyl hydrazides and their derivatives, J. Mol. Struc., 1107 (2016) 99-108.

[21] A. Munir, M. Sirajuddin, M. Zubair, A. Haider, S.A. Tirmizi, S. Ali, H. Khan, K. Ullah, I. Aziz, Synthesis, spectroscopic characterization, and biological screening of levofloxacin based organotin (IV) derivatives, Russ. J. Gen. Chem, 87 (2017) 2380-2390.

[22] F.A. Shah, A.M. Khan, S. Sabir, S. Ali, CTAB–tributylstannic[3-(3′,4′-dichlorophenylamido)propanoate] interaction: a tool for predicting organotin(IV) complex–cell membrane interaction parameters, Colloid. Polym. Sci., 294 (2016) 87-94.

[23] A. Rehman, M.I. Choudhary, W.J. Thomsen, Bioassay Techniques for Drug Development, Harwood Academic Publishers, Amsterdam, The Netherlands, 2001.

[24] B.N. Mayer, N.R. Ferrigni, J.E. Putnam, L.B. Jacobson, D.E. Nichols, J.L. Mclaughlin, Brine shrimp: a convenient general bioassay for active plant constituents, Planta Med. 45 (1982) 31-34.

[25] A. Saeed, P.A. Channar, F.A. Larik, F. Jabeen, U. Muqadar, S. Saeed, U. Flörke, H. Ismail, E. Dilshad, B. Mirza, Design, synthesis, molecular docking studies of organotin-drug derivatives as multi-target agents against antibacterial, antifungal, α-amylase, α-glucosidase and butyrylcholinesterase, Inorg. Chim. Acta, 464 (2017) 204-213.

[26] D.R. Gorja, S. Mukherjee, C.L.T. Meda, G.S. Deora, K.L. Kumar, A. Jain, G.H. Chaudhari, K.S. Chennubhotla, R.K. Banote, P. Kulkarni, K.V. Parsa, Novel N-indolylmethyl substituted olanzapine derivatives: their design, synthesis and evaluation as PDE4B inhibitors. Organic & biomolecular chemistry, *11*(13) (2013), 2075-2079.

[27] G.L. Ellman, K.D. Courtney, V. Andres, R.M. Featherstone, A new and rapid colorimetric determination of acetylcholinesterase activity, Biochemical pharmacology, 7(2) (1961) 88-95.

[28] S.J. Hossan, M. El-Sayed, H. Aoshima, Antioxidative and anti α-amylase activities of four wild plants consumed by nomads in Egypt. Orient. Pharm. Exp. Med., 9(3) (2009) 217-224.

[29] B. Elya, K. Basah, A. Mun'im,W. Yuliastuti, A. Bangun, E.K. Septiana, Screening of *α*-Glucosidase Inhibitory Activity from Some Plants of Apocynaceae, Clusiaceae, Euphorbiaceae and Rubiaceae, J. Biomedi. Biotechnol., 2012 (2012) 1-6.

[30] A.R. Leach, B.K. Shoichet, C. Peishoff, Prediction of protein−ligand interactions. Docking and scoring: Successes and gaps, J. Med. Chem., 49 (2006) 5851-5855.

[31] L. Ming, Z. Wei, W. Jianteng, L. Xiukun, Synthesis and α-glucosidase inhibitory mechanisms of bis (2, 3-dibromo-4, 5-dihydroxybenzyl) ether, a potential marine bromophenol α-glucosidase inhibitor, Mar. Drugs, 9 (2011) 1554-1565.

[32] G.B. Deacon, R.J. Phillips, Relationships between the carbon-oxygen stretching frequencies of carboxylato complexes and the type of carboxylate coordination, Coordination Chemistry Reviews 33 (1980) 227-250.

[33] T. P. Lockhart, W. F. Manders, E. M. Holts, Solution and solid-state molecular structures of $Me_2Sn(OAc)_2$ and its hydrolyzate,$([Me_2Sn(OAc)]_2O)_2$, by solution and solid-state

carbon-13 NMR; X-ray diffraction study of the hydrolyzate, J. Am. Chem. Soc., 108 (1986) 6611-6616.

[34] S. Sadiq-ur-Rehman, M. Ali, M. Mazhar, M. Parvez, catena-Poly [[trimethyltin (IV)]-μ-3-(4-chlorophenyl)-2-phenylpropenoato-κ2O: O′], Acta Crystallogr., Sect. E: Struct. Rep. Online, 60 (2004) m1394–m1396.

[35] M. Sirajuddin, S. Ali, A. Badshah, Drug–DNA interactions and their study by UV–Visible, fluorescence spectroscopies and cyclic voltametry, J. Photochem. Photobio. B, 124 (2013) 1-19.

[36] H.A. Benesi, J.H. Hildebrand, A spectrophotometric investigation of the interaction of iodine with aromatic hydrocarbons, J. Am. Chem. Soc., 71 (1949) 2703-2707.

[37] M. Sirajuddin, N. Uddin, S. Ali, M.N. Tahir, Potential bioactive Schiff base compounds: Synthesis, characterization, X-ray structures, biological screenings and interaction with Salmon sperm DNA, Spectrochim. Acta Part A, 116 (2013) 111-121.

[38] T. Q. Liu, R. Guo, Influence of low cetyltrimethylammonium bromide concentration on the interactions and properties of hemoglobin with acyclovir, Chin. J. Chem., 24 (2006) 620-626.

[39] S. Shah, A. Saeed, Q. Sharif, A study of micellization parameters and electrostatic interactions in micellar solution of sodium dodecyl sulfate, Colloids Surf. A Physicochem. Eng. Asp., 155 (1999) 405-412.

[40] S.B. Ferreira, A.C. Sodero, M.F. Cardoso, E.S. Lima, C. R. Kaiser, F.P. Silva Jr, V.F. Ferreira, Synthesis, biological activity, and molecular modeling studies of 1H-1,2,3-Triazole Derivatives of Carbohydrates as α-Glucosidases Inhibitors, J. Med. Chem., 53 (2010) 2364-2375.

Highlights

- Synthesis of Novel organotin(IV) Carboxylates
- Spectroscopic characterizations by FT-IR, NMR and single crystal X-ray
- Interaction with SS-DNA showing intercalation mode
- Interaction with CTAB (surfactant)
- Inhibition of alpha amylase and alpha glucosidase enzymes
- Molecular docking study strongly supporting the experimental data